

Improved production of $O_2(a^1\Delta)$ in transverse radio-frequency discharges

B. S. Woodard,^a J. W. Zimmerman,^a J. T. Verdeyen,^b D. L. Carroll,^b T. H. Field,^b
G. F. Benavides,^{a,b} A. D. Palla,^b and W. C. Solomon^a

^a Univ. of Illinois at Urbana-Champaign, 104 S. Wright, Urbana, IL 61801

^b CU Aerospace, 2100 Oak St. – Ste 206, Champaign, IL 61820

ABSTRACT

Experimental investigations of radio-frequency discharges in $O_2/He/NO$ mixtures in the pressure range of 1-100 Torr and power range of 0.1-2.5 kW have indicated that $O_2(a^1\Delta)$ production is a strong function of geometry, pressure and diluent ratio. The goal of these investigations was maximization of both the yield and flow rate (power flux) of $O_2(a^1\Delta)$ in order to produce favorable conditions for application to an electric oxygen-iodine laser (EOIL). As pressure is increased, yield performance is dominated by the influence of geometry and diluent ratio. Numerous measurements of $O_2(a^1\Delta)$, oxygen atoms, and discharge excited states are made in order to describe the discharge performance dependence on various parameters.

1. INTRODUCTION

The classical chemical oxygen-iodine laser first reported by McDermott¹ operates on the electronic transition of the iodine atom at 1315 nm, $I(^2P_{1/2}) \rightarrow I(^2P_{3/2})$ [denoted hereafter as I^* and I respectively]. The lasing state I^* is produced by near resonant energy transfer with the singlet oxygen metastable $O_2(a^1\Delta)$ [denoted hereafter as $O_2(a)$]. In typical systems, a chemical two-phase process is used to produce the $O_2(a)$ at the interface of liquid basic H_2O_2 and Cl_2 gas. Zaleskii² and Fournier³ made early studies towards using electric discharges for $O_2(a)$ production to pump iodine for lasing, but were unable to obtain positive gain. More recently, various groups⁴⁻⁹ have investigated similar continuous flowing systems and have measured $O_2(a)$ yields sufficient for positive gain at room temperature. Gain in an electrically-driven system was achieved in work by Carroll *et al.*,¹⁰ with lasing in the same system reported in subsequent work¹¹. This system¹¹ made use of a capacitively-coupled longitudinal 13.56 MHz discharge in $O_2:He$ mixtures to provide energy storage in $O_2(a)$. Since this first reporting of a viable electric discharge-driven oxygen-iodine laser system (called EOIL, ElectricOIL, or DOIL in the literature), there have been a number of other successful demonstrations of gain¹²⁻¹⁴ and lasing.^{13,14} The highest reported gain to date is 0.10 % cm^{-1} with a laser power of 6.2 W.¹⁵

Braginsky *et al.* has shown results regarding pressure-tube diameter scaling in transverse capacitive RF discharges in oxygen. Their research has produced 16% $O_2(a)$ yield at 10 Torr in pure oxygen in a tube with a 14 mm inner diameter.¹⁶ In more recent work, 9% yield was accomplished at 20 Torr in pure oxygen in a 7 mm inner diameter tube.¹⁷ These studies are not directly comparable to the work presented here as they utilize a different RF excitation frequency and have their discharge walls coated with HgO to remove oxygen atoms.¹⁸ However, the idea that smaller discharge tubes are required at high pressure to create large quantities of $O_2(a)$ is a common theme. Moon *et al.* investigated RF discharges in helium at atmospheric pressure and also found that decreasing the electrode gap at high pressure provided desirable conditions such as stable discharges that fill the electrode volume.¹⁹

Optimal production of $O_2(a)$ at a given pressure is a function of geometry of the discharge and the helium diluent ratio. Experimental results (primarily $O_2(a)$ and atomic oxygen yields) are presented herein that illustrate these effects at pressures between 1 and 100 Torr. The general trends observed are:

- i) A decay law for $O_2(a)$ can be deduced that is a function of pressure and flow time from the exit of the discharge.
- ii) As pressure increases, the discharge diameter required for optimal $O_2(a)$ production decreases.
- iii) At 20 Torr, the small diameter discharge tube creates more oxygen atoms than the larger diameter tube while at 50 Torr, the opposite is true.
- iv) Oxygen atoms recombine more rapidly at 50 Torr than at 20 Torr.

- v) At moderate pressure (40 Torr) increased helium diluent can provide high O₂(a) yields even with a large discharge gap although more RF power is required for the peak of the O₂(a) production.

2. EXPERIMENTAL APPARATUS

All the results discussed in this paper were produced using a capacitively coupled transverse RF discharge operating at 13.56 MHz. Four different sized quartz tubes were tested, and with only one exception (clearly noted below), the discharges were all 25.4 cm (10 inches) long. Details of the four discharge tubes are given in Table 1.

Table 1: Transverse RF discharge geometries.

Reference	Internal Diameter	External Diameter	Internal Volume (25.4 cm long)
2"	50 mm	55 mm	499 cm ³
1"	25 mm	29 mm	125 cm ³
3/4"	16 mm	19 mm	51 cm ³
1/2"	9.8 mm	12 mm	19 cm ³

Results from two types of transverse discharges are presented; Fig. 1 illustrates the differences between the “clamshell” and the “parallel plate” discharges. The clamshell discharge consists of a copper foil fitting around the tube that is clamped against a Teflon bar running the length of the discharge. The parallel plate discharge has two 2 mm thick copper sheets held by plastic bolts that clamp the two sheets together. An ENI OEM-25A provided the power for the experiments at 13.56 MHz, and the incident and reflected powers to the radio-frequency (RF) matching network were measured by a Bird Thruline model 43 wattmeter (RF “System Power” is the difference of the incident and reflected powers). Matching the power to the discharge was achieved using a traditional PI-matching network. Micro-Motion CMF and Omega FMA mass flow meters were used to measure the flow rates of the gases. Pressures in the flow tubes were measured with MKS Instruments and Leybold capacitance manometers. The flow setups used in this study are sketched in Fig. 2. The length of glass tubing downstream of the discharge allowed spatial measurements to be made of the O₂(a) and oxygen atoms. When the parallel plate discharge was employed, measurements of the oxygen atom concentration within the discharge could be made as well.

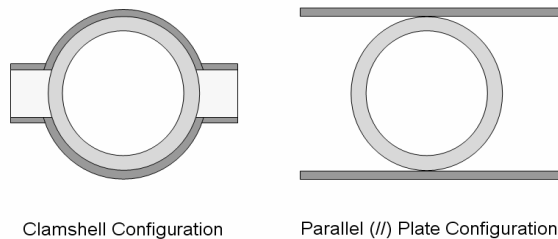


Figure 1: Cross-sectional illustrations of clamshell and parallel plate discharges. Flow is into the paper.

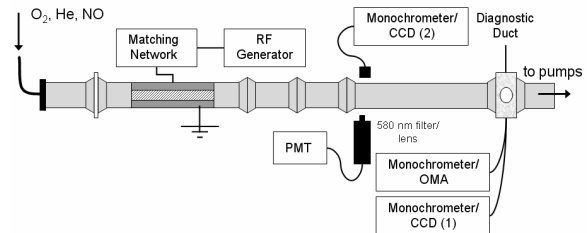
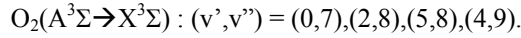
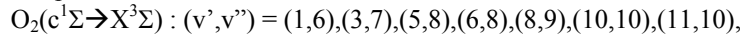


Figure 2: Sketch of experimental apparatus.

A Princeton Instruments/Acton Optical Multi-channel Analyzer (OMA-V, 1024-element InGaAs array) with a 0.3 m monochromator and a 600 g/mm grating blazed at 1 μm was used for measurements at 1268 nm. An Apogee E47 CCD camera coupled to a Roper Scientific/Acton Research 150-mm monochromator (1) was used to measure the emission of O₂(b) at 762 nm to determine flow temperature, as well as the emissions of excited atomic oxygen at 777 nm, and excited argon at 750.4 and 751.5 nm. A Santa Barbara Instruments Group CCD with an Acton 150-mm monochromator (2) was also used to measure O₂(b). The oxygen atom concentration was determined using argon actinometry within the discharge and downstream of the discharge NO₂* emission was employed. Details of determining the oxygen atom concentration from the ratio of excited oxygen and argon states are provided in Zimmerman²⁰ based on techniques employed by Rakhimova *et al.*²¹ The broadband emission of NO₂* was measured using a Hamamatsu R955 photomultiplier with a narrowband 580 nm filter and a 50 mm focal length collection lens; the O-atom concentration was determined from NO₂* using the method described by Piper.²² These optical diagnostics were fiber coupled using either Oriel model #77538 glass fiber bundles or ThorLabs 600 μm x 5 m multimode fibers.

To provide a more precise determination of the volume of the discharge under conditions where the discharge did not fill the entire electrode volume, a measurement of the Herzberg I and II band groups²³ in O₂ was performed using a Nikon D70 with narrowband 404.7 nm filter placed in the optical path. The filter has an 11-nm bandwidth (399-410 nm), which allows capture of



The camera was configured to measure the emission through the quartz tube from the discharge between the high voltage and grounded electrodes.

3. EXPERIMENTAL RESULTS

As the discharge experiments cover a larger range of operating pressures, more care must be taken in order to make appropriate comparisons between data taken at different pressures and diluent flow rates. The decay of the O₂(a) yield appears to be primarily a strong function of the pressure and the time required for a molecule to travel from the exit of the discharge to the measurement location. Data presented in Zimmerman²⁴ provides further details regarding this decay, and Fig. 3 shows that for several pressures that a measure of yield decay follows the same trend.

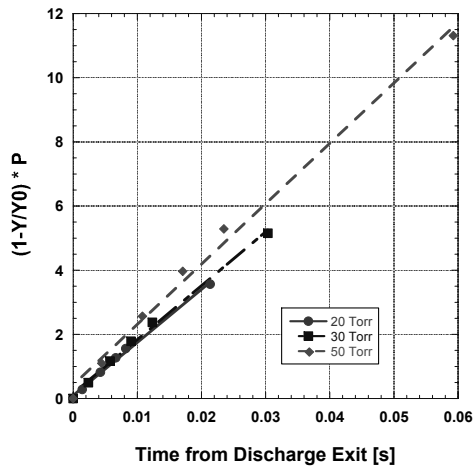


Figure 3: A measure of O₂(a) yield decay vs. flow time from the exit of the discharge for three pressures. Y is the O₂(a) yield at a given time from the discharge exit, and Y₀ is the yield at the discharge exit. P is the pressure.

Equation 1 shows the yield correction derived from the data shown in Fig. 3 that is applied to the data in this work.

$$Y_0 = \frac{Y}{1 - 175.36 \frac{t}{p}} \quad (1)$$

With this calibration, all the O₂(a) yields can be compared as if the measurements were made at the exit of the discharge. This type of correction is necessary to make proper comparisons between different data sets having variable discharge geometries and pressures. For each discharge configuration, the diagnostic duct was a set distance from the exit of the discharge, but as the pressure changed, the velocity changed as well. Ideally one would like to acquire all of the data at the exit of the discharge, however this was experimentally difficult to implement for most of our setups. Therefore, we elected to use this calibration method to translate the data back to the exit of the discharge.

Figure 4 shows the O₂(a) yield as a function of pressure for four different electrode and flow tube configurations with a mixture of 10:33:0.15 mmol/s O₂:He:NO at 800 W. Throughout this work, the “O₂(a) Yield” is defined as [O₂(a)]/[O₂]_{input}(T,p), where [O₂]_{input}(T,p) is the total input O₂ density evaluated at the local measured temperature T and pressure p. For these flow conditions, the highest O₂(a) yield comes from the 2” clamshell discharge at about 20 Torr, but at higher pressures, the performance from the 3/4” discharge is superior. A portion of the reason for this behavior is that the discharge does not fill the 10 inches of discharge length in the 2” tube as the pressure increases. The discharge is pushed back toward the downstream edge of the electrodes. While not shown here, measurements of the Herzberg I and II band groups allow a gauge of the length of the discharge as shown in Zimmerman.²⁴ As the discharge shrinks, the power density increases, and the efficiency of O₂(a) production decreases. In the case of the

smaller discharge tube, the discharge continues to fill the electrode gap at higher pressures. Figure 4 also contains data from a 14" long discharge in a 3/4" tube (triangles) that is 40% longer than the standard 10" length discharge in a 3/4" tube (diamonds). At pressures between 20 and 40 Torr, this added discharge length provides an improvement to the O₂(a) yield because the power density is lower. As the discharge is constricted to shorter than the 10 inch case, the yields are identical since the additional length with no discharge provides no benefit. Data from a 1/2" discharge are shown as well. For these flow conditions, the pressure gradient in the 1/2" tube is greater than in the other discharges, so that may explain its different trend. At pressures greater than 100 Torr, it appears that the 1/2" discharge may provide the best O₂(a) yield, but that yield is still quite low.

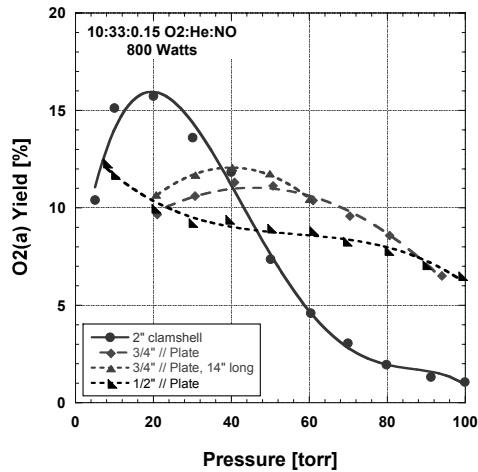


Figure 4: O₂(a) yield vs. pressure for four different discharge electrode gaps/configurations for 10:33:0.15 mmol/s O₂:He:NO at 800 W. The symbol “//” in the legend represents parallel plate configurations.

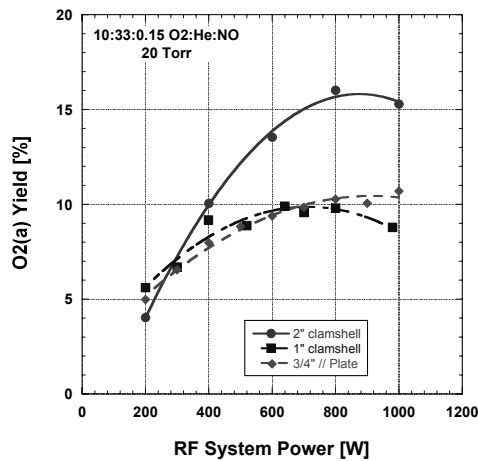


Figure 5: O₂(a) yield vs. RF system power at 20 Torr for three discharge geometries with 10:33:0.15 O₂:He:NO.

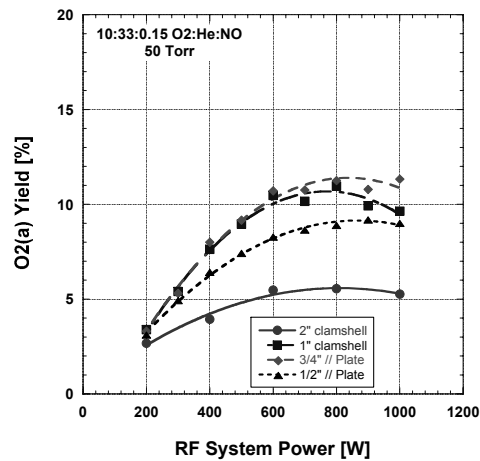


Figure 6: O₂(a) yield vs. RF system power at 50 Torr for four discharge geometries with 10:33:0.15 O₂:He:NO.

Figures 5 and 6 show another dimension of the data discussed for Fig. 4. For the same discharge configurations, pressure was held constant at 20 Torr (Fig. 5) and 50 Torr (Fig. 6) and the RF system power was changed. A 1" clamshell discharge is added to the data set, and the 1/2" discharge was not taken at 20 Torr. In discharge tubes with diameters of 1" or smaller, the difference in O₂(a) production in a clamshell or parallel plate discharge is negligible (not shown for brevity). In the 2" discharge the clamshell performs better at lower pressures (Fig. 5) but worse at higher pressure (Fig. 6). In all the cases shown in Fig. 5 and 6, the yield curves roll over and flatten at a similar power level, but discharge power density plays a role in improving the yield at high pressures. Alumina discharge tubes with the same dimensions as the quartz ones were used to take data similar to Fig. 5 and 6, and the O₂(a) yields were nearly identical (not shown for brevity). Alumina is more robust than quartz and can be machined, so it may be of use in future designs, but all the work presented here utilizes discharges inside quartz tubes.

In order to provide more information about the differences between these discharge geometries, the oxygen atom yields were measured as a function of position inside the discharge region using parallel plate configurations. Figures 7 and 8 contain this information for three discharge geometries at 20 and 50 Torr, respectively. The flow rates are the same (10:33:0.15 mmol/s O₂:He:NO) as the previous cases with the addition of 0.3 mmol/s of Ar in order to make trace argon actinometry possible. The RF power in these cases is a constant of 800 W.

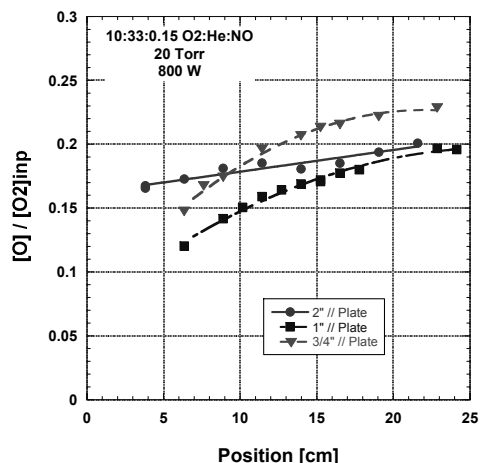


Figure 7: Oxygen atom yield vs. position in the discharge for three different geometries at 20 Torr for 10:33:0.15 mmol/s O₂:He:NO at 800 W.

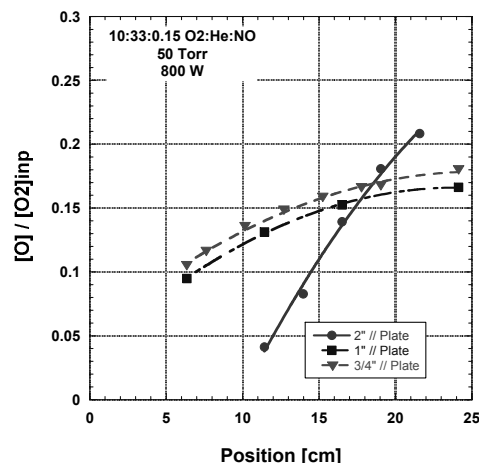


Figure 8: Oxygen atom yield vs. position in the discharge for three different geometries at 50 Torr for 10:33:0.15 mmol/s O₂:He:NO at 800 W.

The oxygen atom yield is defined similarly to the O₂(a) yield in that oxygen atom concentration is divided by the oxygen input density evaluated at the local temperature and pressure. In Fig. 7, all three geometries fill the electrodes, so the 3/4" configuration has the highest power density which results in the largest oxygen atom production. However, in Fig. 8 at 50 Torr, wall recombination of oxygen atoms dominates, and the 3/4" discharge produces less oxygen atoms than the 2" discharge. At 50 Torr, the 2" discharge does not fill the electrode volume which explains the lack of oxygen atoms upstream of 11 cm.

The flow rate of NO also has a large impact on the oxygen atom yield within the discharge. Figures 9 and 10 contain data that show this effect for the case of 10:33 mmol/s O₂:He at 20 Torr and 800 W for the 2" and 3/4" parallel plate discharges, respectively. The data shown is for NO flow rates of 0, 0.1, and 0.3 mmol/s.

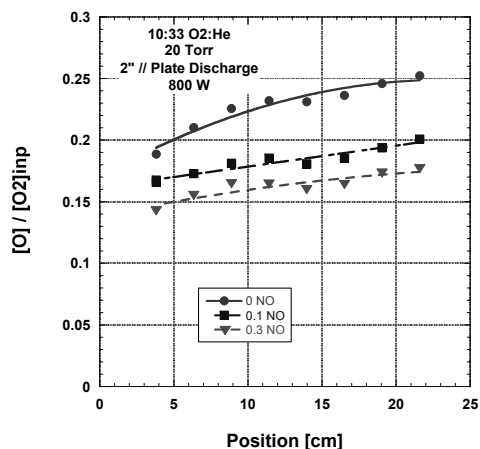


Figure 9: Oxygen atom yield vs. position in the 2" parallel plate discharge for three NO flow rates at 20 Torr for 10:33 mmol/s O₂:He at 800 W.

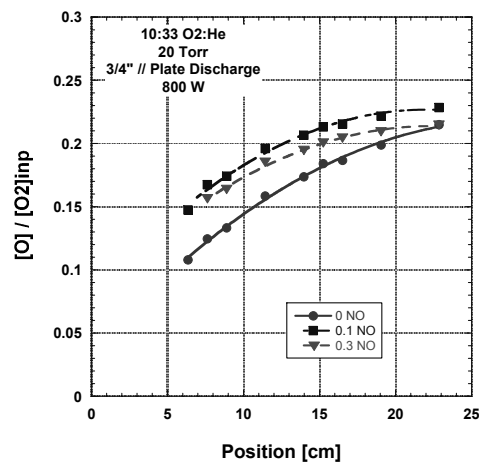


Figure 10: Oxygen atom yield vs. position in the 3/4" parallel plate discharge for three NO flow rates at 20 Torr for 10:33 mmol/s O₂:He at 800 W.

The trend shown in Fig. 9 follows the expected pattern. The oxygen atom concentration is significantly decreased with the addition of some NO. Increasing the NO flow rate further does reduce the atoms more, but the effect is smaller even for a larger increase in NO flow rate. The data from the smaller discharge, however, does not show the same tendency. Figure 10 shows that the initial addition of NO actually increases the atom concentration before it decreases with more NO. We believe this is a flow velocity (or residence time) effect. The depletion of oxygen atoms with NO requires time for the two step process to work as discussed in Kaufman.²⁵ The flow velocity is approximately ten times as fast in the $\frac{3}{4}$ " discharge compared to the 2" discharge, so the concentration of NO must be higher in order to see the effect within the discharge. Downstream of the discharge, the oxygen atoms decay faster at higher pressure as Fig. 11 illustrates.

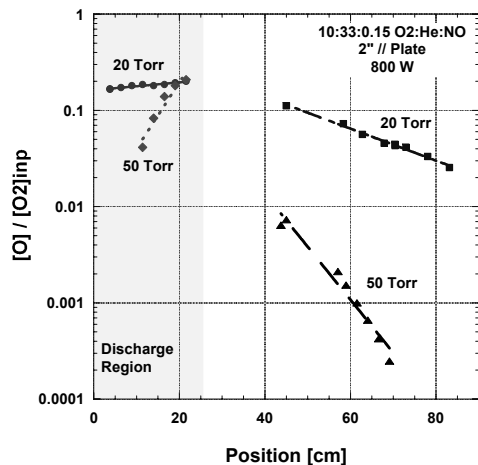


Figure 11: Oxygen atom yield vs. position in and downstream of the 2" parallel plate discharge for two pressures for 10:33:0.15 mmol/s O₂:He:NO at 800 W.

The variation with distance is plotted for both 20 and 50 Torr for the 2" clamshell discharge at 800 W with 10:33:0.15 mmol/s O₂:He:NO. The atomic yield is shown on a logarithmic scale in Fig. 11, and by 20 cm from the exit of the discharge, the 50 Torr concentration has already dropped by an order of magnitude. Oxygen atom yield versus distance plots suffer from the problem that time elapsed from entrance to the discharge to measurement location varies with geometry and pressure, but a scaling law for the atoms was not clear from the data as it was for the O₂(a) yield, Eq 1.

Helium diluent also plays a critical role in maximizing the O₂(a) yield especially at high pressures. Figure 12 shows the O₂(a) yield, oxygen atom yield, and temperature versus helium flow rate at 20 Torr and 700 W for the 2" clamshell discharge. This oxygen flow rate, pressure, and power have been baseline operating conditions for our EOIL system for about two years.

Oxygen atom concentrations in this section were determined by NO₂* emission. The O₂(a) yield peaks around 1:4 O₂:He. The flow temperature decreases significantly with higher flow rates of helium due to increased thermal transport properties of the gas mixture. At 50 Torr in the $\frac{3}{4}$ " discharge, more helium is required to maximize the O₂(a) yield for a higher oxygen flow rate, Fig. 13. The oxygen flow rate was held at 5, 10, and 15 mmol/s, and the power was held such that each case has a power loading of 70 J/mmol of O₂. The flow of NO was 0.15 mmol/s in all cases, and the O₂(a) yield peaks at different O₂:He ratios for the different cases. This information led to the high O₂(a) yield data in Fig. 14. The O₂(a) and oxygen atom yields are shown versus pressure for 3:60 O₂:He at 800 W and 5:100 O₂:He at 1200 W. The NO flow rate is constant at 0.15 mmol/s, and these data were acquired at the exit of the 2" clamshell discharge. The O₂(a) yield peaks at 26% at 40 Torr for the 3 mmol/s of oxygen case although the yield is only slightly lower in the 5 mmol/s of oxygen case. These high helium diluent ratios cause the discharge to produce a large concentration of oxygen atoms especially at low pressure, but at 50 Torr, the concentration is comparable to the baseline EOIL level.

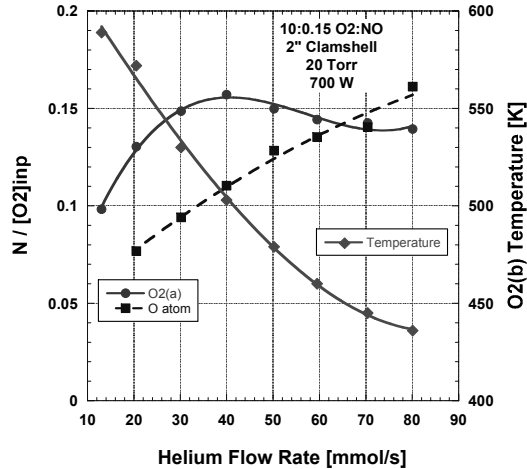


Figure 12: $O_2(a)$ yield, oxygen atom yield, and temperature vs. helium flow rate at 20 Torr for 10:0.15 mmol/s $O_2:NO$ at 700 W in a 2" clamshell discharge.

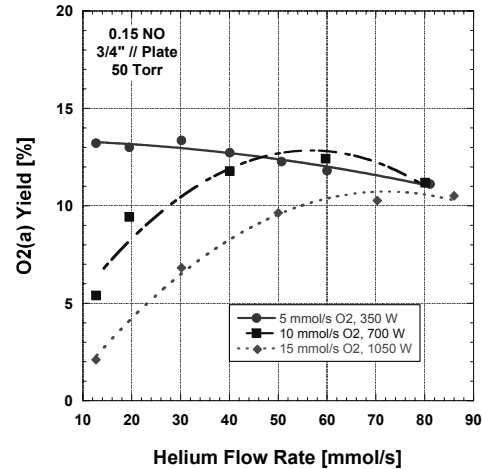


Figure 13: $O_2(a)$ yield vs. helium flow rate for three O_2 flow rates at 50 Torr with 0.15 mmol/s NO while keeping 70 J/mmol O_2 in a 3/4" parallel plate discharge.

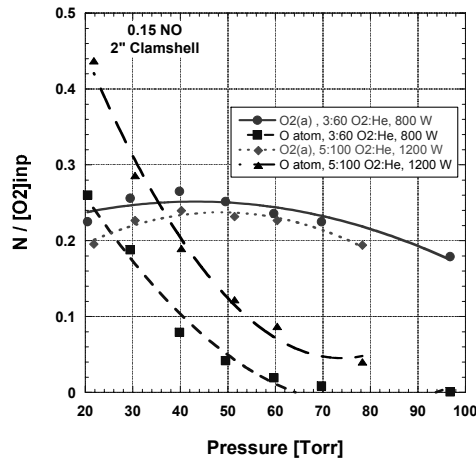


Figure 14: $O_2(a)$ yield and oxygen atom yield vs. pressure for 3:60 mmol/s $O_2:He$ at 800 W and 5:100 mmol/s $O_2:He$ at 1200 W with 0.15 mmol/s NO in a 2" clamshell discharge.

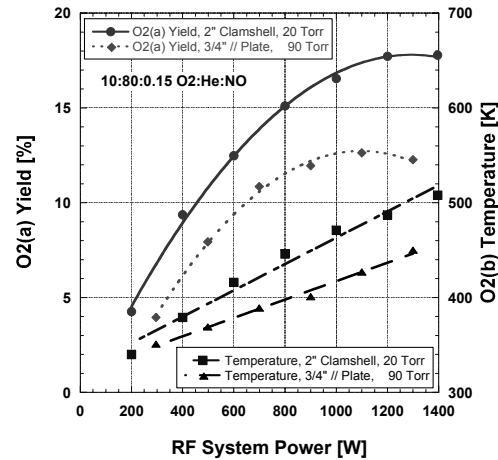


Figure 15: $O_2(a)$ yield and temperature vs. RF system power for 10:80:0.15 mmol/s $O_2:He:NO$ at 20 Torr in a 2" clamshell discharge and 90 Torr in a 3/4" parallel plate discharge.

Even at 90 Torr, the $O_2(a)$ yield is almost 13% for a high diluent ratio (1:8 $O_2:He$) as illustrated in Fig. 15. The 3/4" parallel plate discharge was used, and the flow rates were 10:80:0.15 mmol/s $O_2:He:NO$. Note that this information was collected approximately 84 cm downstream from the discharge exit. The yield has been corrected, but the temperature represents the temperature at the measurement location. Figure 15 also includes data taken with the 2" clamshell discharge at 20 Torr for the same flow rates. By diluting the standard 10 mmol/s of oxygen at 20 Torr with more helium, the $O_2(a)$ yield increases from 16% to 18% although significantly more RF power is required in the 1:8 $O_2:He$ case.

Figure 16 shows another dimension of the data from Fig. 14. The $O_2(a)$ yield is plotted versus RF system power for 3, 5, and 7 mmol/s of oxygen keeping the diluent ratio 1:20 $O_2:He$ with 0.15 mmol/s NO at 40 Torr using the 2" clamshell discharge. The baseline EOIL case of 10:33:0.15 $O_2:He:NO$ at 20 Torr is also included. Let us now consider the amount of power stored in the $O_2(a)$. Using Eq. 2, the data from Fig. 16 can be converted to Fig. 17.

$$\dot{n}_{O_2} \left[\frac{\text{mmol} / \text{s}}{1000} \right] \times Y_{O_2(a)} \left[\frac{\%}{100} \right] \times N_A \times \text{energy} \left[\frac{0.98 \text{ eV}}{O_2(a) \text{ molecule}} \times \frac{1.602 \times 10^{-19} \text{ J}}{\text{eV}} \right] = O_2(a) \text{ Power} [W] \quad (2)$$

where N_A is Avogadro's number, \dot{n}_{O_2} is the molar flow rate of oxygen, and Y is the $O_2(a)$ yield. While the yields shown in Fig. 16 for these high diluent ratio cases are higher, the oxygen flow rates are decreased, so as Fig. 17 illustrates, the amount of power in the $O_2(a)$ state is not necessarily as high as the baseline case. The conditions for Fig. 16 and 17 are identical. Clearly, both high yields and high oxygen flow rates are required to produce large $O_2(a)$ powers, and the 7:140 mmol/s O_2 :He at 40 Torr case produces similar powers to the baseline case which occurs at half the pressure; these conditions will be explored further in future work.

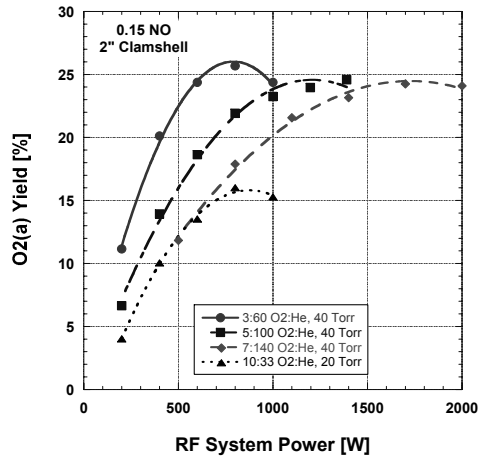


Figure 16: $O_2(a)$ yield vs. RF system power for 1:20 O_2 :He at 40 Torr and ~1:3 O_2 :He at 20 Torr with 0.15 mmol/s NO in a 2'' clamshell discharge.

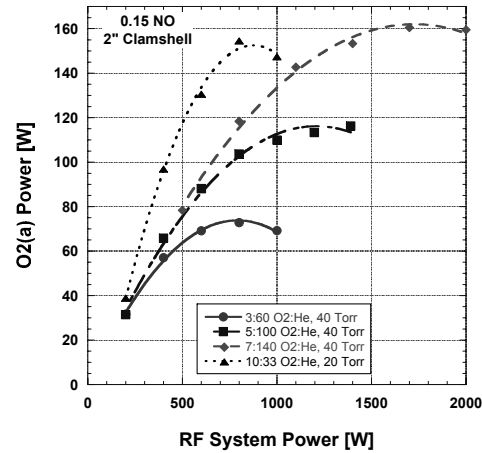


Figure 17: $O_2(a)$ Power vs. RF system power for 1:20 O_2 :He at 40 Torr and ~1:3 O_2 :He at 20 Torr with 0.15 mmol/s NO in a 2'' clamshell discharge.

4. CONCLUSIONS

Geometry and diluent ratio are critical parameters for the production of high $O_2(a)$ yields from transverse RF discharges at moderate pressures (50-100 Torr). The discharge that effectively makes $O_2(a)$ at 20 Torr does not fill the electrode volume as the pressure increases, and this effect leads to decreased yield. By shortening the gap between the electrodes, the discharge fills the volume at higher pressures and more effectively creates $O_2(a)$ at those pressures. At the same time, increasing the helium diluent in the discharge also increases the $O_2(a)$ yield at higher pressure. Yields over 25% are measured with 1:20 O_2 :He in the discharge. Future work must exploit both of these effects to create a discharge capable of producing high yields with high oxygen flow rates to produce a flow with high $O_2(a)$ power.

ACKNOWLEDGMENTS

This work was supported by the Missile Defense Agency (MDA) through the U.S. Army Space and Missile Defense Command (USA SMDC). The authors gratefully thank: B. Otey (USA SMDC); W.T. Rawlins and S.J. Davis (Physical Sciences Inc.); M.C. Heaven (Emory Univ.); J. Kotora and D. Podolski (MDA); and G.W. Sutton (Sparta Inc.). They would also like to thank D.M. King and J.K. Laystrom for their technical assistance.

REFERENCES

1. W. McDermott, N. Pchelkin, D. Benard, and R. Bousek, *Appl. Phys. Lett.* **32** (8) 469 (1978).
2. Zalesskii, V. Yu., *Zh. Eksp. Teor. Fiz.*, **67** 30 (1974) [*Sov. Phys. JETP* **40** (1) 14 (1975)].
3. G. Fournier, J. Bonnet, and D. Pigache, *J. Physique* **41** Colloque C9, 449 (1980).
4. D.L. Carroll, J.T. Verdeyen, D.M. King, B.S. Woodard, L.W. Skorski, J.W. Zimmerman, and W.C. Solomon, *IEEE J. Quant. Elect.* **39** (9) 1150 (2003).
5. D.L. Carroll, J.T. Verdeyen, D.M. King, B.S. Woodard, J.W. Zimmerman, L.W. Skorski, and W.C. Solomon, "Recent Experimental Measurements of the ElectricOIL System," AIAA Paper 2003-4029 (2003).

6. J. Schmiedberger, S. Hirahara, Y. Ichinoche, M. Suzuki, W. Masuda, Y. Kihara, E. Yoshitani, and H. Fujii, *SPIE Vol. 4184*, 32 (2001).
7. A.E. Hill, in *Proc. of the International Conf. on Lasers 2000*, ed. by V. Corcoran and T. Corcoran (STS Press, McClean, VA) 249 (2001).
8. A.A. Ionin, Y.M. Klimachev, A.A. Kotkov, I.V. Kochetov, A.P. Napartovich, L.V. Seleznev, D.V. Sinitsyn, and G.D. Hager, *J. Phys. D: Appl. Phys.* **36** 982 (2003).
9. T.V. Rakhimova, A.S. Kovalev, A.T. Rakhimov, K.S. Klopovsky, D.V. Lopaev, Y.A. Mankelevich, O.V. Proshina, O.V. Braginsky, and A.N. Vasilieva, "Radio-Frequency Plasma Generation of Singlet ($a^1\Delta_g$) Oxygen in O_2 and O_2 :Ar (He) Mixtures," AIAA Paper 2003-4306 (2003).
10. D.L. Carroll, J. T. Verdeyen, D. M. King, J. W. Zimmerman, J. K. Laystrom, B. S. Woodard, N. Richardson, K. Kittell, M.J. Kushner, and W. C. Solomon, "Measurement of positive gain on the 1315 nm transition of atomic iodine pumped by $O_2(a^1\Delta)$ produced in an electric discharge," *Appl. Phys. Lett.*, **85** (8) 1320-1322 (2004).
11. D.L. Carroll, J. T. Verdeyen, D. M. King, J. Zimmerman, J. Laystrom, B. Woodard, G. Benavides, K. Kittell, D. Stafford, M. J. Kushner, and W. C. Solomon, "Continuous-wave laser oscillation on the 1315 nm transition of atomic iodine pumped by $O_2(a^1\Delta)$ produced in an electric discharge," *Appl. Phys. Lett.*, **86**, 111104 (2005).
12. Rawlins, W.T., Lee, S., Kessler, W.J., and Davis, S.J., "Observations of Gain on the $I(^2P_{1/2} \rightarrow ^2P_{3/2})$ Transition by Energy Transfer from $O_2(a^1\Delta_g)$ Generated by a Microwave Discharge in a Subsonic Flow Reactor," *Appl. Phys. Lett.* **86**, 051105 (2005).
13. Verdeyen, J. T., Carroll, D. L., King, D. M., Laystrom, J. K., Benavides, G. F., Zimmerman, J. W., Woodard, B. S., and Solomon, W. C., "Continuous-wave laser oscillation in subsonic flow on the 1315 nm atomic iodine transition pumped by electric discharge produced $O_2(a^1\Delta)$," *Appl. Phys. Lett.*, **89**, 101115 (2006).
14. Hicks, A., Tirupathi, S., Jiang, N., Utkin, Yu., Lempert, W. R., Rich, J. W., and Adamovich, I. V., "Design and operation of a supersonic flow cavity for a non-self-sustained electric discharge pumped oxygen-iodine laser," *J. Phys. D: Appl. Phys.*, **40**, 1408-1415 (2007).
15. Benavides, G. F., Zimmerman, J. W., Woodard, B. S., Carroll, D. L., Verdeyen, J. T., Field, T. H., Palla, A.D. and Solomon, W. C., "Gain and continuous-wave laser power enhancement with a secondary discharge to predissociate molecular iodine in an electric oxygen-iodine discharge," *Appl. Phys. Lett.*, **92**, 041116 (2008).
16. Braginsky, O. V., Kovalev, A. S., Lopaev, D. V., Mankelevich, Yu. A., Proshina, O. V., Rakhimova, T. V., Rakhimov, A. T., and Vasilieva, A. N. "Discharge singlet oxygen generator for oxygen-iodine laser: I. Experiments with rf discharges at 13.56 and 81MHz," *J. Phys. D: Appl. Phys.* **39** 5183-90 (2006).
17. Braginsky, O.V., Kovalev, A.S., Lopaev, D.V., Proshina, O.V., Rakhimova, T.V., Rakhimov, A.T., and Vasilieva, A.N., "Pressure scaling of an electro-discharge singlet oxygen generator (ED SOG)," *J. Phys. D: Appl Phys.* **40** 6571-82 (2007).
18. Proshina, O. V., Rakhimova, T. V., Braginsky, O. V., Kovalev, A. S., Lopaev, D. V., Mankelevich, Yu. A., Rakhimov, A. T., and Vasilieva, A. N., "Discharge singlet oxygen generator for oxygen-iodine laser: II. Two-dimensional modeling of flow oxygen rf plasma at 13.56 and 81MHz power frequency," *J. Phys. D: Appl. Phys.* **39** 5191-200 (2006).
19. Moon, S.Y., Rhee, D.B., Kim, D.B., and Choe, W., " α , γ , and normal, abnormal glow discharge modes in radio-frequency capacitively coupled discharges at atmospheric pressure," *Physics of Plasmas* **13**, 033502 (2006).
20. Zimmerman, J.W., King, D.M., Palla, A.D., Verdeyen, J.T., Carroll, D.L., Laystrom, J.K., Benavides, G.F., Woodard, B.S., Solomon, W.C., Rawlins, W.T., Davis, S.J., and Heaven, M.C., "Important kinetic effects in the hybrid ElectricOIL system." *SPIE Vol. 6261*, 62611R (2006).
21. Rakhimova, T. V., Kovalev, A. S., Lopaev, D. V., Proshina, O. V., Mankelevich, Yu. A., Vasilieva, A. N., Braginsky, O. V., Klopovsky, K. S., Popov, N. A., Rakhimov, A. T., Kolobyanin, Yu. V., "Pressure scaling of an electro-discharge singlet oxygen generator (ED SOG)." *Gas Flow, Chemical Lasers, and High-Power Lasers*, SPIE paper 634608-1 (2006).
22. Piper, L.G., Caledonia, G.E., Kennealy, J.P., *J. Chem. Phys.* **75**, 2847 (1981).
23. Rosen, B. "Spectroscopic Data Relative to Diatomic Molecules." Pergamon Press (French), 424-425 (1970).
24. Zimmerman, J.W., Woodard, B.S., Verdeyen, J.T., Carroll, D.L., Field, T.H., and Solomon, W.C., "Improved production of $O_2(a^1D)$ in capacitively-coupled radio-frequency discharges," *SPIE Vol. 6874-9* (2008).
25. Kaufman, F. *Proc. Roy. Soc. A*, **247**, 123-39 (1958).